

Ligand-Specific Transcriptional Mechanisms Underlie Aryl Hydrocarbon Receptor-Mediated Developmental Toxicity of Oxygenated PAHs

B. C. Goodale,^{*,†} J. La Du,^{*} S. C. Tilton,^{*,‡} C. M. Sullivan,^{*,§} W. H. Bisson,^{*} K. M. Waters,[‡] and R. L. Tanguay^{*,1}

^{*}Department of Environmental and Molecular Toxicology, The Environmental Health Sciences Center, Oregon State University, Corvallis, Oregon 97330; [†]Department of Microbiology and Immunology, Geisel School of Medicine at Dartmouth, Hanover, New Hampshire 03755; [‡]Computational Biology and Bioinformatics, Pacific Northwest National Laboratory, Richland, Washington 99354; [§]Center for Genome Research and Biocomputing, Oregon State University, Corvallis, Oregon 97330

¹To whom correspondence should be addressed at Department of Environmental and Molecular Toxicology, The Environmental Health Sciences Center, Oregon State University, Corvallis, Oregon 97330. Fax: 541-737-6074. E-mail: robert.tanguay@oregonstate.edu

ABSTRACT

Polycyclic aromatic hydrocarbons (PAHs) are priority environmental contaminants that exhibit mutagenic, carcinogenic, proinflammatory, and teratogenic properties. Oxygen-substituted PAHs (OPAHs) are formed during combustion processes and via phototoxidation and biological degradation of parent (unsubstituted) PAHs. Despite their prevalence both in contaminated industrial sites and in urban air, OPAH mechanisms of action in biological systems are relatively understudied. Like parent PAHs, OPAHs exert structure-dependent mutagenic activities and activation of the aryl hydrocarbon receptor (AHR) and cytochrome p450 metabolic pathway. Four-ring OPAHs 1,9-benz-10-anthrone (BEZO) and benz(a)anthracene-7,12-dione (7,12-B[a]AQ) cause morphological aberrations and induce markers of oxidative stress in developing zebrafish with similar potency, but only 7,12-B[a]AQ induces robust Cyp1a protein expression. We investigated the role of the AHR in mediating the toxicity of BEZO and 7,12-B[a]AQ, and found that knockdown of AHR2 rescued developmental effects caused by both compounds. Using RNA-seq and molecular docking, we identified transcriptional responses that precede developmental toxicity induced via differential interaction with AHR2. Redox-homeostasis genes were affected similarly by these OPAHs, while 7,12-B[a]AQ preferentially activated phase 1 metabolism and BEZO uniquely decreased visual system genes. Analysis of biological functions and upstream regulators suggests that BEZO is a weak AHR agonist, but interacts with other transcriptional regulators to cause developmental toxicity in an AHR-dependent manner. Identifying ligand-dependent AHR interactions and signaling pathways is essential for understanding toxicity of this class of environmentally relevant compounds.

Key words: OPAH; zebrafish; aryl hydrocarbon receptor; RNA-seq; benzanthrone; benz(a)anthracene-7,12-dione

Polycyclic aromatic hydrocarbons (PAHs) are priority environmental contaminants in air and at hazardous waste sites. Automobile, wood burning, coal-based energy production, and other combustion processes produce both parent (unsubstituted) PAHs, consisting of multiple fused carbon rings, as well as substituted derivatives. PAHs are associated with both the

gaseous and ultrafine particulate fractions of urban air, can accumulate in the lungs when inhaled, and are considered major carcinogenic components of combustion emissions (Bostrom *et al.*, 2002; Ramirez *et al.*, 2011). Oxygenated, nitrated, and methylated PAHs also form from parent PAHs through photo-oxidation reactions as well as biotic metabolism in the

environment (Lundstedt *et al.*, 2007). The USEPA identified 28 PAHs on its priority pollutant list, based on their prevalence at Superfund sites and potential health effects (USEPA, 2015). Parent PAHs are routinely measured in order to estimate total PAH contamination levels and potential hazard, but degradation products, such as oxygen-substituted PAHs (OPAHs), are less frequently accounted for. As detection methods have improved and standards are more widely available, studies have found that OPAHs are present in PAH-contaminated environmental samples, potentially at higher concentrations than parent PAHs (Layshock *et al.*, 2010; Lundstedt *et al.*, 2006; Walgraeve *et al.*, 2010). Like a number of parent PAHs, some OPAHs are mutagenic (Durant *et al.*, 1996), but little data are available about their toxicity. Toxicological effects of parent PAHs include developmental, cardiac, and immune system disruption mediated by the aryl hydrocarbon receptor (AHR). Substituted PAH structures are likely to also induce toxicological effects beyond mutagenicity in a structure-dependent manner. A screen of OPAH toxicity in developing zebrafish demonstrated that OPAHs cause developmental toxicity at a wide range of waterborne concentrations, with structural elements likely explaining their differential induction of morphological abnormalities (Knecht *et al.*, 2013). Some OPAHs induced expression *cyp1a* via activation of the AHR, and induced the expression of genes involved in redox and response to oxidative stress. While morphological effects of some OPAHs were accompanied by tissue-specific *Cyp1a* expression, others did not induce *Cyp1a*, suggesting AHR-independent toxicity. Because of their ubiquity, and potentially greater prevalence in some environmental situations than parent PAHs, there is a need to understand mechanisms by which OPAHs cause toxicity.

Here we compare the transcriptional signatures and proposed toxicological mechanisms of 2 structurally related OPAHs, 1,9-benz-10-anthrone (BEZO) and benz(a)anthracene-7,12-dione (7,12-B[a]AQ) during embryonic development. These 4-ring OPAHs, which are detected in environmental samples, differ in their ring arrangement and oxygenation pattern. BEZO is detected in air samples associated with high traffic emissions, but is also an important intermediate used in production of dyes currently used in fabrics (Nielsen *et al.*, 1999; Svedman *et al.*, 2014). Exposure has been associated with hepatic and dermal lesions in workers, as well as ascorbic acid depletion in animal models (Singh *et al.*, 2003). It was recently shown to have immunomodulatory effects in mice (Tewari *et al.*, 2015). 7,12-B[a]AQ is also detected in air and at industrial waste sites, and was among the most abundant OPAHs detected in urban air in Beijing (Wang *et al.*, 2011; Wei *et al.*, 2012). 7,12-B[a]AQ can be formed from benz(a)anthracene (BAA), an EPA priority pollutant PAH which is mutagenic and induces developmental toxicity via the AHR (Incardona *et al.*, 2006).

Both BEZO and 7,12-B[a]AQ were identified in a zebrafish toxicity screen to disrupt normal development, while differentially inducing *Cyp1a* protein expression, suggesting distinct modes of action (Knecht *et al.*, 2013). While *Cyp1a* is induced by PAHs that activate the AHR, it does not mediate their developmental effects in zebrafish. We investigated the role of AHR2, the zebrafish homolog with best functional conservation with human AHR, in mediating developmental toxicity of BEZO and 7,12-B[a]AQ. We show that, unexpectedly, developmental effects of both OPAHs require AHR2. Because the genes downstream of AHR2 responsible for PAH-mediated developmental toxicity are not yet known, we further investigated mechanisms of BEZO and 7,12-B[a]AQ toxicity with RNA-seq. Transcriptional profiling sheds light on conserved mechanisms and disrupted

transcripts to consider along with *cyp1a* when inferring exposure and AHR activation by OPAHs. Understanding the multitude of AHR interactions is important for assessing and predicting health risks posed by this class of emerging contaminants.

MATERIALS AND METHODS

Chemicals. Analytical grade (>98% purity) BEZO was purchased from Fluka, and 7,12-B[a]AQ was purchased from Sigma-Aldrich. Compounds were dissolved to 10 mM in dimethyl sulfoxide (DMSO). Stocks were sonicated in a bath sonicator for 15 min before each use. For embryo exposures, BEZO and 7,12-B[a]AQ stocks in 100% DMSO were dissolved in embryo media to a final concentration of 1% DMSO.

Molecular modeling and docking. The homology models of human AHR and zebrafish AHR2-PASB ligand binding domain were built as previously described (Gerlach *et al.*, 2014; Perkins *et al.*, 2014). TCDD, BEZO, 7,12-B[a]AQ, BAA, BAP, anthracene (ANTH), and SP600125 were docked into the models, as reported (Perkins *et al.*, 2014).

Fish husbandry. All experiments were conducted with wild-type 5D or *cyp1a* reporter line Tg(*cyp1a:nls-egfp*) zebrafish. Adult zebrafish were maintained at the Sinnhuber Aquatic Research Laboratory on a recirculating system with a water temperature of $28 \pm 1^\circ\text{C}$, and a 14 h light:10 h dark photoperiod. All experiments were conducted with embryos collected in the morning from multiple adult zebrafish set up for group spawning as described previously (Reimers *et al.*, 2006). Adult care and reproductive techniques were conducted according to Institutional Animal Care and Use Committee protocols at Oregon State University.

OPAH exposure and developmental toxicity assessment. Embryos were cleaned, developmentally staged, and batch-exposed in glass vials at 6 h postfertilization (hpf) to 5, 7.5, and 10 μM concentrations of OPAH or 1% DMSO vehicle control, 20 embryos per vial in 2 ml exposure solution (Kimmel *et al.*, 1995). DMSO was necessary for these exposures because of low solubility of OPAHs, and did not disrupt normal development of our control animals. It may, however, influence gene expression profiles. Vials were incubated at 28°C in the dark on a rocker on lowest setting for the duration of the exposure. Embryos were collected at 48 hpf for RNA and immunohistochemical analysis. For developmental toxicity evaluations, embryos remained in solution until 72 hpf, when they were rinsed 3 times, transferred to individual wells of a 96-well plate, and incubated in fresh embryo media until evaluation at 120 hpf. Embryos were then euthanized with MS-222 (tricaine methanesulfonate) and evaluated for axis, trunk, somite, yolk sac, fin, cardiac, eye, jaw, otic vesicle, brain, and pigment malformations as previously described (Truong *et al.*, 2011). Mortality and the percentage of embryos with each malformation were calculated for each treatment group with the vial (20 embryos) as the experimental unit. Representative larvae were imaged at 48 and 120 hpf with a Nikon Coolpix 5000 digital camera. Developmental toxicity experiments were performed 3 times, and percent incidence data across the 3 replicates were analyzed for significance by 2-way ANOVA with Tukey's all pairwise post hoc test in R.

Morpholino injection. Embryos were injected at the single cell stage with a fluorescein-tagged translation-blocking morpholinos targeting Ahr2 (*ahr2*-MO, 5'TGTACCGATACCCGCCGACAT

GGTT3'), or a standard nonsense control (c-MO, 5'CCTCTT ACCTCAGTTACAATTATA3') purchased from Gene Tools (Philomath, Oregon) at a concentration of 0.75 mM. Injection volume was ~2 nl. Fertilized, normally developing embryos were screened for morpholino incorporation at 4 hpf by fluorescence microscopy. Embryos with evenly incorporated morpholino were batch-exposed to BEZO, 7,12-B[a]AQ, or control, 20 embryos per vial, as described for developmental toxicity and qRT-PCR experiments.

RNA isolation. Groups of 20 embryos were homogenized at 48 hpf in RNazol (Molecular Research Center, Cincinnati, Ohio) using a bullet blender with 0.5 mM zirconium oxide beads (Next Advance, Averill Park, New York). Samples were stored at -80°C until RNA isolation via phenol guanidine extraction. RNA was quantified and quality assessed using a SynergyMx microplate reader with the Gen5 Take3 module to calculate O.D. 260/280 ratios. For the RNA-seq study, 3 biological replicates were collected per treatment group. For qRT-PCR experiments, 4 biological replicates were collected from c-MO and ahr2-MO injected embryos.

Quantitative RT-PCR. cDNA was synthesized from total RNA using the ABI high-capacity cDNA synthesis kit, diluted in water, and 50 ng equivalents of RNA were used for qRT-PCR reactions. Gene-specific primers (MWG Operon) for qRT-PCR amplification are listed in [Supplementary Table S1](#). All qRT-PCR assays were performed in 20 µl reactions consisting of 10 µl Power SYBR Green PCR master mix (Applied Biosystems), 0.4 µl each primer, 9.2 µl H₂O, and 50 ng equivalents of cDNA. Amplification (Step One Plus, Applied Biosystems) was performed with cycling parameters as follows: 95°C for 10 min; 40 cycles of 95°C for 15 s, 60°C for 1 min. A melt curve was performed at 3° increments to assess for multiple products; all primers amplified a single product with comparable efficiency (90–100%). Relative fold change (FC) values in PAH-treated samples compared with vehicle controls were calculated for genes of interest, normalized to β -actin, by the method described by Pfaffl (2001). Four biological replicates were assessed and statistically analyzed by 2-way ANOVA with Tukey's post hoc test.

Immunofluorescence and imaging. Whole embryos were fixed at 48 hpf in 4% paraformaldehyde at 4°C overnight. Mouse α fish CYP1A monoclonal (1:500 dilution, Biosense laboratories) primary antibody and Alexafluor 594 goat α mouse IgG (H+L) (1:1000 dilution, Molecular Probes, Eugene, Oregon) secondary antibody were used for immunofluorescent labeling of Cyp1a as described by Svoboda et al. (2001). Briefly, embryos were washed in phosphate-buffered saline containing 0.1% Tween-20 (PBST), permeabilized by a 1-h incubation in distilled water followed by 20 min in cold acetone and 30 min incubation in 1 mg/ml collagenase. Embryos were blocked for 1 h in PBST with 10% normal goat serum, incubated with 1° antibody in 10% NGS overnight at 4°C, washed in PBST, and incubated in 2° antibody 4 h at RT. Embryos were imaged by epi-fluorescence microscopy using a Zeiss Axiovert 200M microscope with $\times 5$ objective. Immunofluorescence images were created from z-stacks of five 20 µm slices captured with 1.59-s exposure time. Two overlapping frames were spliced to capture the entire length of each larva. In order to visualize tissue location of cyp1a expression in cyp1a reporter fish, representative GFP fluorescent images were collected using a Zeiss Axiovert 200M microscope with $\times 10$ objective with 2×2 binning. Camera exposure time for 7,12-B[a]AQ 48 hpf fish was 336 ms. Dampened cyp1a signal in BEZO

and control fish required increasing camera exposure times to 894 and 1429 ms. Images were taken at 72 hpf with increasing exposure times of 277, 1260, and 3260 ms for 7,12-B[a]AQ, BEZO, and controls, respectively.

Paired-end mRNA sequencing. Total RNA was isolated from groups of 20 embryos using methods described above and RNA integrity was confirmed (RIN score >9) with an Agilent Bioanalyzer 2100. Total RNA samples were sent to University of Oregon Genomics Core Facility for library preparation and sequencing. mRNA was poly-A selected with the Dynabeads mRNA purification kit (Invitrogen), and sequencing libraries prepared with the ScriptSeq v2 kit with ScriptSeq index primers. Paired-end sequencing (50 bp) was conducted with an Illumina HiSeq 2000 sequencer and sequence files were transferred to the Oregon State University Center for Genome Research and Biocomputing for analysis. Sequences were filtered based on Illumina quality scores and analyzed for quality using FastQC analytical software (Babraham Bioinformatics). Read ends were trimmed to exclude low-quality sequences. Sequencing data and processing details are available in the NCBI Gene Expression Omnibus (GSE68666).

Sequence mapping, transcriptome assembly, and statistical analysis. Paired-end sequence reads were aligned with TopHat version 2.0.7 (Trapnell et al., 2009) to Danio rerio genome assembly Zv9.70 with min/max intron length 50/10 000 bp, only allowing for paired alignments (—no-mixed option). The percentage of reads mapped ranged from 74 to 76% for all samples, resulting in 35–60 million mapped reads per sample for further analysis. Read counts per gene were calculated using Htseq-count using the —intersection-nonempty parameter (Anders et al., 2014). Unexpressed genes, defined as genes with a sum of <50 total mapped reads across all samples, were then filtered from further analysis. Sample library sizes were normalized in edgeR using a trimmed mean of M values (TMM, where $M = \log_2$ fold change). Differential expression was determined in edgeR using the using the Cox-Reid profile-adjusted likelihood (CR) method to calculate dispersions, fitting negative binomial generalized linear models (GLM), and using the GLM likelihood ratio test (Robinson et al., 2010). All P-values presented were adjusted for false discovery rate using the Benjamini-Hochberg method, $P < .05$ was used to identify genes differentially expressed (DE) in BEZO or 7,12-B[a]AQ exposure groups compared with control. Moderated log-counts-per-million values were calculated in edgeR for bidirectional hierarchical clustering using Pearson's distance metric. Heatmaps were generated in R using dendroextras and heatplus packages.

Pathway analysis. The R GO-Seq package was used to identify enriched Gene Ontology (GO) terms from clusters of genes in the BEZO-7,12-B[a]AQ heatmap (Young et al., 2010). GO terms with an FDR-corrected P value < .05 were considered significant. The Bioinformatics Resource Manager v 2.3 (BRM) was used to identify Entrez IDs and human homologs of significant genes identified in our statistical comparison using the Zv9 transcriptome (Tilton et al., 2012). We used Metacore GeneGo software to identify enriched biological processes, GO terms, and predicted transcription factors (TFs) from the BEZO and 7,12-B[a]AQ significant gene lists ($P < .05$). Statistical significance of over-connected interactions was calculated using a hypergeometric distribution, where the P-value represents the probability of a particular mapping arising by chance for experimental data compared with the background (Nikolsky et al., 2009). MetaCore processes

TABLE 1. Predicted Docking Scores of 7,12-B[a]AQ, BEZO and Selected AHR Agonists in Human AHR and Zebrafish AHR2

	TCDD	ANTH	BAA	7,12-B [a]AQ	SP600125	BaP	BEZO
Zebrafish AHR2	-21.86	-14.64	-13.95	-8.5	-6.7 ^a	-4.88	-2.2
Human AHR	-26.38	-13.52	-17.34	-17	-7.66 ^a	-6.76	-5

^aAverage score obtained from the individual docking of the 2 existing tautomers of SP600125.

and predicted TFs were filtered to include only those associated with at least 10 genes in the dataset. We report MetaCore processes with enrichment P values $<1.0e-3$. TFs with P values $<5.0e-7$ were considered significant. Networks were constructed in MetaCore for experimental data using an algorithm that identifies the shortest path to directly connect nodes in the dataset to TFs. Network visualizations were generated in Cytoscape (Shannon et al., 2003).

RESULTS

BEZO and 7,12-B[a]AQ Are Predicted to Bind the AHR With Different Affinities

In a previous study, 7,12-B[a]AQ caused developmental toxicity and induced robust Cyp1a expression in developing zebrafish. BEZO also caused developmental toxicity at concentrations below 20 μ M, but Cyp1a protein was not detected in BEZO-exposed larvae (Knecht et al., 2013). Because of the lack of Cyp1a induction, we hypothesized that BEZO exposure disrupted development via a mechanism independent of the AHR. We conducted molecular docking to determine whether BEZO and 7,12-B[a]AQ are predicted to bind the human AHR- and zebrafish AHR2-PASB ligand binding domains and to exert an agonist effect. We compared the OPAHs with potent AHR agonist 2,3,7,8-tetrachlorodibenzo-*p*-dioxin (TCDD), partial agonist 1,9-pyrazoloanthrone (alias SP600125), and parent PAHs ANTH, BAA, and benzo(a)pyrene (BaP). With these models, the more negative the docking score, the higher the AHR binding and activation. TCDD docked with the highest scores in both zebrafish AHR2 (-21.86) and human AHR (-26.38) as previously reported (Table 1) (Gerlach et al., 2014; Perkins et al., 2014). Three and four ring PAHs ANTH and BAA ranked second and third. The OPAH 7,12-B[a]AQ had similar predicted binding to the AHR as parent PAH BAA, which was previously shown to be an AHR agonist (Incardona et al., 2006). Interestingly, anthrone derivative SP600125, which was previously identified as a partial agonist of the AHR, docked in human AHR and zebrafish AHR2 with slightly higher affinity than BaP (Table 1) (Dvorak et al., 2008). BEZO was predicted to bind both the human AHR and zebrafish AHR2, but with the lowest affinity of compounds tested (Table 1). Taken together, these results predict 7,12-B[a]AQ and BEZO to bind and activate both the human AHR and zebrafish AHR2. While 7,12-B[a]AQ ranked among other 4–5 ring PAHs that are experimentally validated AHR agonists, BEZO was predicted to be a weak, partial agonist of the AHR, with further studies required for a complete pharmacological characterization.

BEZO and 7,12-B[a]AQ-Induced Developmental Toxicity Is Dependent on the AHR

The molecular docking study predicted that 7,12-B[a]AQ would induce AHR-mediated toxicity similar to other AHR agonists. BEZO was predicted to be a partial/weak AHR agonist, many of which induce toxicity independent of AHR2 (Brown et al., 2015).

We investigated the role of the AHR in 7,12-B[a]AQ and BEZO-induced developmental toxicity by knocking down AHR2 during development. We exposed *ahr2* and control morpholino-injected (morphant) zebrafish embryos to a range of OPAH concentrations previously demonstrated to disrupt development at 120 hpf (Knecht et al., 2013). We sought to identify exposure concentrations that consistently induced malformations but not mortality, to allow for mechanistic comparison between OPAHs. The concentrations tested (5–10 μ M) are not meant to mimic environmental exposures, as direct comparison between systems is complicated by low compound solubility in water and potential loss to exposure vessels. Both 7,12-B[a]AQ and BEZO induced a concentration-dependent increase in the percent of control morphant embryos with axis, trunk, brain, yolk sac, circulation, pericardial edema, eye, and jaw malformations (Fig. 1A, solid lines). Neither compound caused significant mortality at 120 hpf (Fig. 1A). We did not observe significant increases in fin, pigment, somite, or otic vesicle malformations with exposure to either OPAH (data not shown). Malformation profiles induced by the 2 OPAHs were of similar severity at the 10 μ M concentration (Figs. 1A, solid lines, 1C and 1D). As expected for an AHR agonist, AHR2 knockdown prevented pericardial edema and other malformations induced by 7,12-B[a]AQ (Figs. 1A, dashed lines, and 1F). Surprisingly, AHR2 knockdown also protected against pericardial edema and other developmental effects induced by BEZO (Figs. 1A, dashed lines, and 1G). While a slight increase in embryos exhibiting at least 1 malformation was observed in AHR2 morphants exposed to 7,12-B[a]AQ or BEZO, the increases were not significant (2-way ANOVA, $P < .05$). From these data we conclude that BEZO and 7,12-B[a]AQ induce AHR2-dependent developmental toxicity with similar potency, despite their differences in AHR binding affinity.

BEZO and 7,12-B[a]AQ Induce Distinct Malformations and Cytochrome P450 1A Expression During Early Development

Although we found BEZO and 7,12-B[a]AQ caused similar, AHR2-dependent malformations at 120 hpf, previous research showed they induced dramatically different expression levels of *cyp1a*, a widely used biomarker of AHR activation (Knecht et al., 2013). To further investigate this apparent contradiction, we examined *cyp1a* mRNA expression over multiple early developmental time points, and investigated the dependence of *cyp1a* mRNA and protein expression on AHR2. Differences in uptake or metabolism kinetics could affect the timing of Cyp1a induction by 7,12-B[a]AQ and BEZO, resulting in misleading differences at a single time point. We measured *cyp1a* expression via qRT-PCR at 12, 19, 24, and 30 hpf to determine whether the difference in *cyp1a* induction between the OPAHs was consistent over time. At 12 hpf (6 h postexposure), 7,12-B[a]AQ had already induced a ~30-fold increase in *cyp1a* expression, while *cyp1a* in BEZO exposed embryos was not significantly different from controls (Fig. 2A). For both compounds, the highest level of *cyp1a* expression was observed at 24 hpf, where 7,12-B[a]AQ induced a 165-fold change (FC), compared with a 4-FC induced by BEZO. Cyp1a expression followed a similar trajectory for both compounds, declining slightly at 30 and 48 hpf, with 7,12-B[a]AQ induction remaining significantly higher than BEZO. We therefore found no evidence of early AHR activity or rapid metabolism underlying the difference in *cyp1a* profiles induced by these OPAHs at single time points.

We focused further investigation at 48 hpf, when robust Cyp1a protein expression can be visualized with immunofluorescence, but the liver and its metabolic activity are not yet

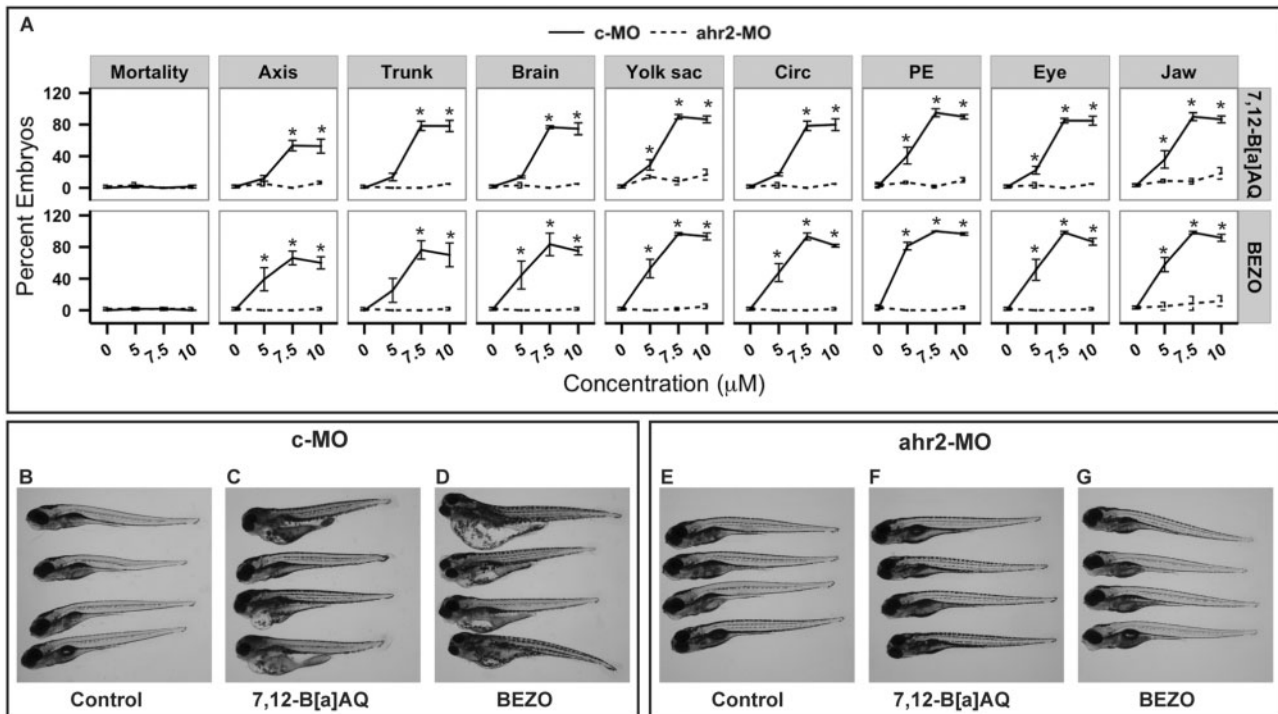


FIG. 1. Developmental toxicity of 7,12-B[a]AQ and BEZO at 120 hpf is AHR2-dependent. **A**, Exposure from 6 to 72 hpf to 5, 7.5, and 10 μ M 7,12-B[a]AQ or BEZO did not cause significant mortality at 120 hpf, but both OPAHs induced concentration-dependent increases in the percent of control morpholino(MO)-injected larvae with axis, trunk, somite, yolk sac, circulatory (Circ), pericardial (PE), eye, and jaw abnormalities (solid lines). 7,12-B[a]AQ or BEZO exposure did not cause any significant malformations above control levels in *ahr2*-MO-injected embryos (dashed lines). Data represent 3 independent replicates of 20 embryos per treatment group and were analyzed by 2-way ANOVA. *Significantly different than control $P < .05$. **B–D**, Representative images of control-MO-injected embryos exposed to 1% DMSO vehicle control, 10 μ M 7,12-B[a]AQ, and 10 μ M BEZO, respectively. Severe malformations including pericardial edema, yolk sac edema, craniofacial malformations, and eye defects can be observed in (C) and (D). **E–G**, Representative images of *ahr2*-MO-injected embryos exposed to 1% DMSO vehicle control, 10 μ M 7,12-B[a]AQ, and 10 μ M BEZO, respectively, show rescue of morphological abnormalities.

functional. We measured *cyp1a* mRNA expression in control and *ahr2* morphants, and found that AHR2 knockdown reduced the 201-fold increase in *cyp1a* expression induced by 7,12-B[a]AQ by ~75%, to a 56-fold induction (Fig. 2B). The significant induction of *cyp1a* in AHR2 morphants compared with unexposed controls could be a result of incomplete knockdown with the morpholino, or activation of one of the other zebrafish AHR isoforms. While we are not able to distinguish between these mechanisms in this study, we note that AHR2 knockdown was sufficient to protect against toxicity (Fig. 1). AHR2 knockdown similarly ameliorated *cyp1a* induction by BEZO (Fig. 2B).

We used immunofluorescence to visualize Cyp1a protein expression in 48 hpf larvae. Cyp1a was highly expressed throughout the vasculature in control morphants exposed to 7,12-B[a]AQ (Fig. 2C). Only faint Cyp1a protein expression was observed in AHR2 morphants exposed to 7,12-B[a]AQ (Fig. 2D). While we cannot rule out activation of *Ahr1a* or *Ahr1b* in this study, Knecht et al. (2013) showed complete absence of Cyp1A induction by 7,12-B[a]AQ in AHR2 mutant embryos, which suggests that the Cyp1a observed in AHR2 morphants is a result of incomplete knockdown with the AHR2 morpholino. In contrast to 7,12-B[a]AQ, BEZO did not induce Cyp1a protein expression detectable by immunofluorescence in control or *ahr2* morphants (Fig. 2E, *ahr2* morphants not shown). Cyp1a was not observed in control or *ahr2* morphants exposed to DMSO (Fig. 2F, *ahr2* morphants not shown).

AHR agonists, including TCDD and other PAHs, induce Cyp1a expression in the developing heart (Carney et al., 2004; Incardona et al., 2011). Constitutive AHR activation in the

myocardium is sufficient to lead to a cascade of developmental effects recapitulating TCDD exposure, but developmental effects of AHR activation are not mediated by Cyp1a (Carney et al., 2004; Lanham et al., 2014). We were not able to distinguish developmental effects of BEZO and 7,12-B[a]AQ at 120 hpf, when severe secondary effects had developed. At 48 hpf, however, phenotypic differences were observed between larvae exposed to the 2 OPAHs. In control morphants, 7.5 μ M 7,12-B[a]AQ induced developmental abnormalities, including pooling of blood ventral to the developing heart, slight curved body axis and reduced size, which were apparent by 48 hpf (Fig. 3A, compared with Fig. 3E vehicle control). More severe edema was observed in control morphants exposed to BEZO (Fig. 3C). These early effects were not observed in AHR2 morphants (Figs. 3B and 3D). Because BEZO induced a small but significant increase in *cyp1a* mRNA, we further investigated AHR activation indirectly in the Tg(*cyp1a:nls-egfp*) transgenic reporter fish to determine whether *cyp1a* was expressed in a highly tissue-specific manner not detectable by our *cyp1a* immunofluorescence method. The *cyp1a* reporter line harbors a fosmid construct with GFP under control of a recombiner zebrafish *cyp1a* promoter, and recapitulates *cyp1a* induction by TCDD with high sensitivity (Kim et al., 2013). We exposed *cyp1a* reporter zebrafish from 6 to 48 hpf to 10 μ M 7,12-B[a]AQ, 10 μ M BEZO or 1% DMSO and imaged at 48 hpf, or washed and grew out to 72 hpf. Exposure to 7,12-B[a]AQ induced strong expression in heart and vasculature similar to previous immunofluorescence results at 48 hpf (Fig. 3G, compared with Fig. 2C). Only by increasing camera exposure time from 336 ms, used for 7,12-B[a]AQ, to 894 and

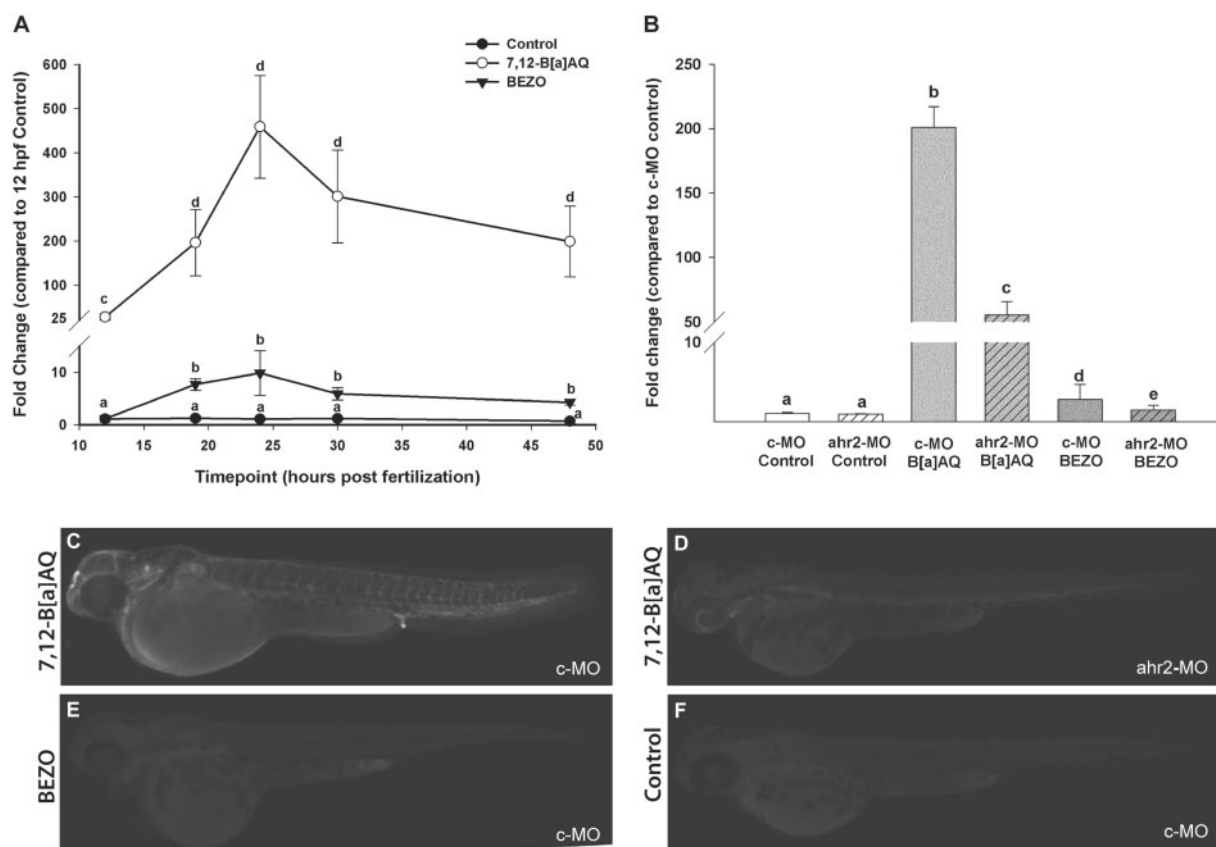


FIG. 2. Differential Cyp1a induction by 7,12-B[a]AQ and BEZO is dependent on AHR2. **A**, Exposure to 7.5 μ M 7,12-B[a]AQ, or BEZO-induced differential expression of *cyp1a* mRNA at 12, 19, 24, 30, and 48 hpf. Both BEZO and 7,12-B[a]AQ significantly induced *cyp1a* expression compared with the DMSO control. However, 7,12-B[a]AQ caused a stronger effect by an order of magnitude, which was significantly different from BEZO ($P < .05$). Data represent 3 independent biological replicates analyzed by 2-way ANOVA with Tukey's *post hoc* test, significantly different expression is designated with different letters ($P < .05$). **B**, Exposure to 7,12-B[a]AQ induced *cyp1a* expression in control morpholino (cmo, solid bars) injected embryos, which was significantly decreased in *ahr2* morphants (*ahr2*mo, hashed bars). BEZO induced a 4-fold increase in *cyp1a* expression, which was also significantly decreased in *ahr2* morphants. Data represent 4 biological replicates analyzed by 2-way ANOVA with Tukey's *post hoc* test. Significantly different induction is designated with different letters ($P < .05$). **C**, Immunofluorescent labeling of Cyp1a protein in 48 hpf embryo exposed to 7,12-B[a]AQ showed strong fluorescence throughout the vasculature. **D**, Cyp1a protein was largely absent in *ahr2*mo-injected embryos exposed to 7,12-B[a]AQ. **E**, **F**, No Cyp1a protein expression was visible in BEZO exposed c-MO or *ahr2*-MO embryos. **F**, **G**, No Cyp1a protein expression was visible in control (DMSO exposed) c-MO or *ahr2*-MO embryos at 48 hpf.

1429 ms, we were able to detect *cyp1a* in BEZO and control exposed embryos, respectively, primarily surrounding the otic vesicle and in the skin. We obtained similar results at 72 hpf, when *cyp1a* expression was clearly observed in the vasculature and hearts of 7,12-B[a]AQ exposed larvae, but detected in the head and developing gills of BEZO and Controls only with longer exposure time (Supplementary Fig. S1).

Together these studies show that BEZO causes early developmental effects, including pericardial edema that are dependent on AHR2. Unlike other AHR agonists, such as TCDD and BAA, BEZO causes these AHR2-dependent effects without simultaneously inducing robust Cyp1a expression. We cannot rule out the possibility that *cyp1a* mRNA is expressed in BEZO exposed embryos but is not translated to protein. While *cyp1a* is a well-known downstream target of AHR, it does not mediate developmental toxicity of AHR agonists such as TCDD (Carney et al., 2004). Indeed, Cyp1a can have a protective effect against toxicity induced by PAHs (Brown et al., 2015).

Transcriptional Profiling With RNA-seq

The large difference in *cyp1a* expression in embryos exposed to BEZO and 7,12-B[a]AQ at an EC100 concentration for malformations, suggested differences in AHR-mediated transcriptional

regulation. To further investigate these differences, we used RNA-seq to identify genes DE in embryos exposed to BEZO or 7,12-B[a]AQ from 6 to 48 hpf. Three biological replicates of pooled RNA from 20 embryos were sequenced for each exposure group. In embryos exposed to 7,12-B[a]AQ, we identified 2270 genes DE with an FDR-corrected P value $< .05$ compared with control (Supplementary Table S2). In BEZO-exposed embryos, 1532 genes were significantly DE (Supplementary Table S3). Just over 50% of these were unique to BEZO, while 732 genes were significantly affected by both BEZO and 7,12-B[a]AQ. We focused comparative functional analysis on the 462 significantly DE genes with >2 FC compared with control (Fig. 4A). Of these genes, only 82 were similarly affected by both OPAHs.

This partial overlap in significant targets could reflect activation of different molecular pathways, or activation of the same pathway with different potency; venn comparisons of significant gene lists ignore magnitude or direction of gene regulation. To visualize gene expression changes induced by BEZO and 7,12-B[a]AQ, we conducted bidirectional hierarchical clustering of DE genes with FC >2 , and found that samples clustered tightly by exposure group (Fig. 4B). Genes were divided into 7 clusters with distinct expression patterns across exposure groups, which suggest that the OPAHs affect different molecular

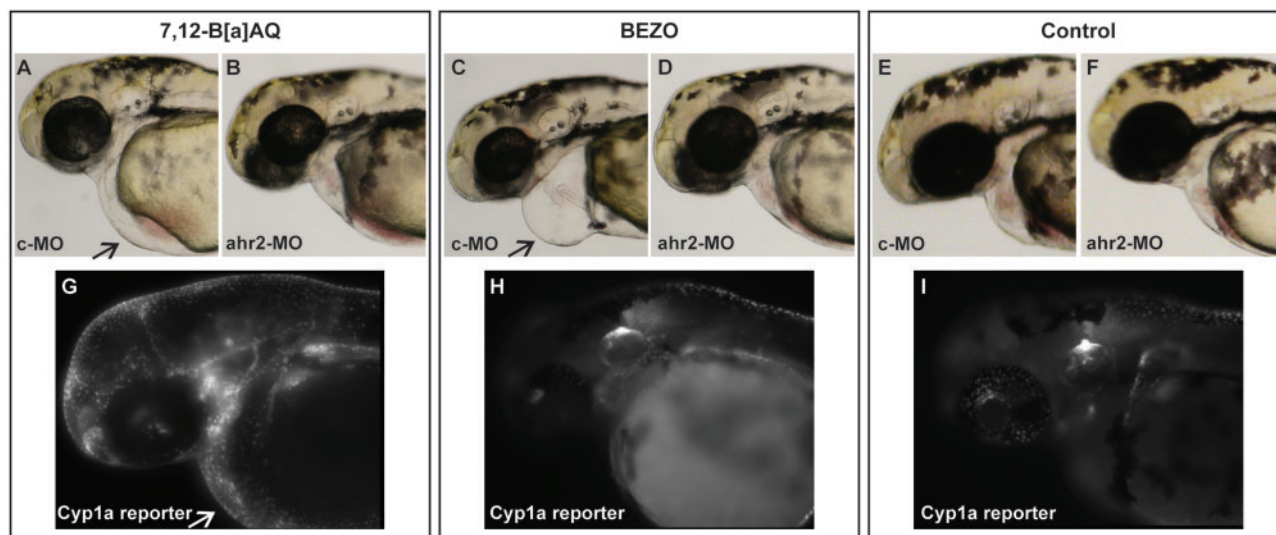


FIG. 3. Disrupted cardiac morphology at 48 hpf is preceded by differential *cyp1a* induction in 7,12-B[a]AQ and BEZO exposed embryos. A, Representative light microscope image of control-injected 48 hpf embryo exposed to 7.5 μ M 7,12-B[a]AQ. Pooling of blood is noted with arrow. B, Representative light microscope image of ahr2-MO injected 48 hpf embryo exposed to 7.5 μ M 7,12-B[a]AQ. C, 48 hpf embryo exposed to 7.5 μ M BEZO. Pericardial edema is noted with arrow. D, Representative light microscope image of ahr2-MO injected 48 hpf embryo exposed to 7.5 μ M BEZO. E, F 48 hpf control-injected and ahr2-MO-injected embryos exposed to 1% DMSO vehicle control. G, At 48 hpf, *cyp1a* reporter embryos exposed to 10 μ M 7,12-B[a]AQ, showed strong fluorescence throughout the vasculature and heart (336 ms exposure). H, With increasing camera exposure times, yolk syncytial layer, otic vesicle, and limited vasculature is seen in 10 μ M BEZO (894 ms exposure). I, DMSO controls had dim expression in skin and otic vesicle (1429 ms exposure).

pathways. We identified GO functions for each cluster using GoSeq, and report GO terms that were enriched with an FDR-corrected P value $< .05$. Genes that decreased most in response to 7,12-B[a]AQ (Fig. 4B, pink cluster) were more likely to have endopeptidase or inorganic anion transport than would be expected by chance. By contrast, genes that were strongly down-regulated by BEZO, but not 7,12-B[a]AQ (Fig. 4B, yellow cluster), were significantly enriched for visual perception and transporter functions. Genes with the largest FCs in this cluster (>8 -fold decrease) were *ngnt2b*, *opsin 1 long wave 1*, and *gamma-crystallin2d11*. Also in this cluster were short wave opsins (*opn1sw1* and *opn1sw2*) retinoschisin 1, retina and anterior neural fold homeobox 1 and 13 other gamma crystalline genes, the majority of which are located together on chromosome 9. A third large cluster of transcripts was elevated by both OPAHs, but more highly by 7,12-B[a]AQ, and was associated with cellular response to xenobiotic stimulus and iron ion binding (Fig. 4B, orange cluster). The genes with the largest FCs in this cluster (>16 -fold increase with 7,12-B[a]AQ) were *cyp1a*, *wfikkn1*, *cyp1c1*, *zgc:173962* (glutathione S-transferase alpha 1 homolog), *cyp1c2*, *ahrrb*, and *fgf7*.

We validated expression of genes from several clusters using qRT-PCR and measured comparable expression changes using qRT-PCR and RNA-seq (Supplementary Table S4). Induction of *ctsl1*, *sult6b1*, and *cxc4* by the 2 compounds was similar. Because *ctsl1* has previously shown to be responsive to the AHR in humans, we investigated its expression over development as a potential alternative biomarker of AHR-mediated developmental toxicity (Mbewe-Campbell et al., 2012). qRT-PCR analysis confirmed induction of *ctsl1* by both BEZO and 7,12-B[a]AQ at 48 hpf. However, endogenous expression in control animals increased dramatically by 72 hpf, and was no different between control and 7,12-B[a]AQ-exposed embryos at 96 hpf, suggesting it may not be a reliable biomarker in the context of development (Supplementary Fig. S2).

AHR2 Knockdown Prevents Increases in BEZO and 7,12-B[a]AQ-Specific Transcripts

In addition to binding the AHR, OPAHs and/or metabolites interact with other targets that could mediate AHR-independent transcriptional changes, potentially leading to the difference in transcriptional profiles induced by BEZO and 7,12-B[a]AQ. We selected a set of DE transcripts from the RNA-seq dataset and investigated their expression in control and ahr2 morphants exposed to 7.5 μ M BEZO or 7,12-B[a]AQ. Cytochrome p450 1b1 (*cyp1b1*) and WAP, follistatin/kazal, immunoglobulin, kunitz, and netrin domain containing 1 (*wfikkn1*) were among the top 10 genes increased by 7,12-B[a]AQ in the RNA-seq analysis, and were increased to a lesser extent by BEZO. We confirmed these increases in control morphants exposed to 7,12-B[a]AQ, and found AHR2 knockdown prevented induction of these genes (Figs. 5A and 5B). Glutathione S-transferase pi 2 (*gstp2*) is a redox responsive gene that was also elevated by both OPAHs in the RNA-seq analysis. qRT-PCR confirmed significant induction by both 7,12-B[a]AQ (4.8-fold) and BEZO (3.1-fold) in control morphants, but no significant induction was observed in ahr2 morphants (Fig. 5C). We next investigated BEZO-induced transcripts from our RNA-seq analysis. The expression of insulin-like growth factor binding protein 1a (*igfbp1a*) was significantly different than control for both OPAHs, but more highly expressed in embryos exposed to BEZO. Arginase2 (*arg2*) was significantly elevated by BEZO but unchanged by 7,12-B[a]AQ. These differential expression patterns were confirmed by qRT-PCR in the control morphants, and AHR2 knockdown prevented induction of both *igfbp1* and *arg2* (Figs. 5D and 5E). Finally, we investigated p53 expression, as a master regulator that was elevated by BEZO in the RNA-seq dataset. A slight (1.2-fold) induction was detected by qRT-PCR, with no significant difference between 7,12-B[a]AQ and BEZO. Ahr2 morphants had slightly higher p53 expression than control morphants, which was not affected by OPAH exposure (Fig. 5F).

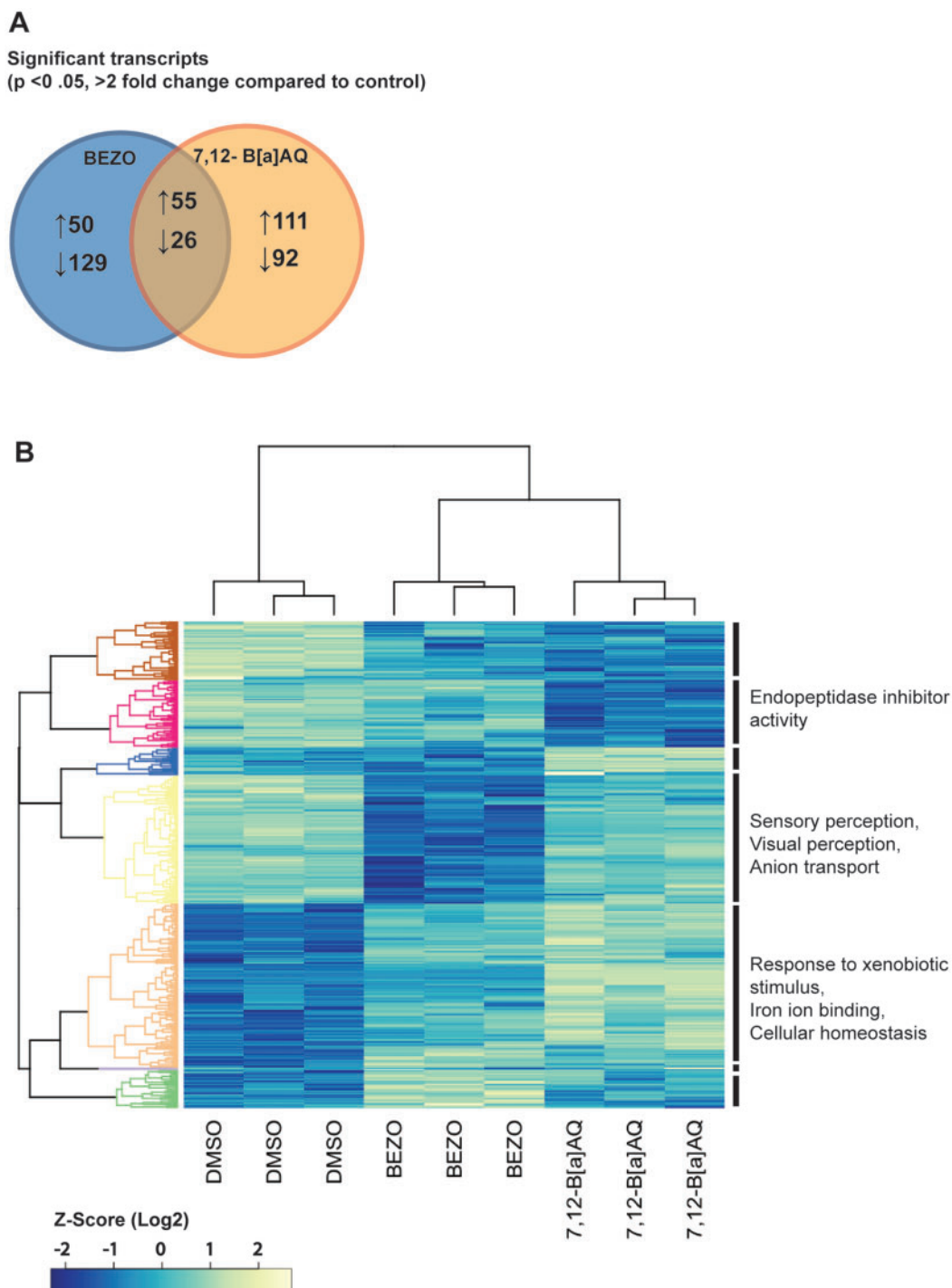


FIG. 4. BEZO and 7,12-B[a]AQ differentially modulate genes involved in metabolism and photoreceptor development. A, Comparison of significantly DE genes (FDR-corrected P value $< .05$, $FC > 2$) in BEZO and 7,12-B[a]AQ exposed embryos compared with control. B, Bidirectionally clustered heatmap of the union of transcripts significantly DE in BEZO or 7,12-B[a]AQ embryos compared with control (FDR-corrected P value $< .05$, $FC > 2$). Significantly enriched GO terms were identified for 3 of the transcript clusters.

BEZO and 7,12-B[a]AQ Regulated Transcripts Are Involved in Visual System and Immune Development

In order to leverage biological knowledge from mammalian models in our interpretation of genes disrupted by BEZO and 7,12-B[a]AQ during development, we used the Bioinformatic Resource Manager to identify homologs of zebrafish transcripts from our RNA-seq analysis. Human or mouse Entrez IDs

(human homolog preferred) were identified for 432 of the 462 DE genes. We then used Metacore GeneGo software to identify significant biological networks and transcriptional regulators associated with the BEZO and 7,12-B[a]AQ significant gene lists, and identified 13 biological processes enriched at a significance level of $P < .001$. We compared the OPAHs, and found that the most significantly enriched process, Visual perception was

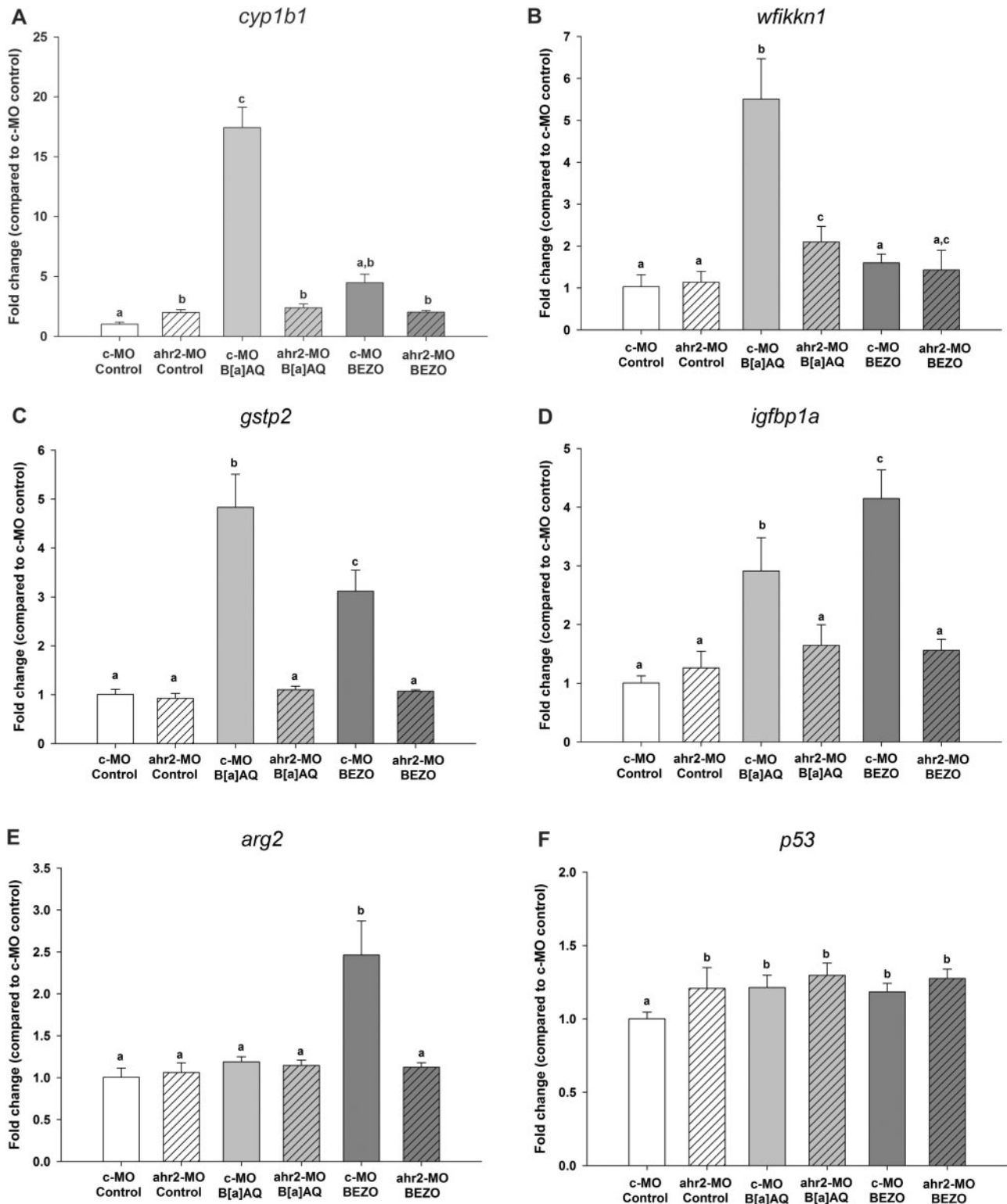


FIG. 5. qRT-PCR analysis of OPAH targets in control and AHR2 morphants. Exposure to 7.5 μ M 7,12-B[a]AQ or BEZO-induced differential expression of *cyp1b1* (A), *gstp2* (B), *arg2* (C), *igfbp1a* (D), *ponzr4* (E), and *p53* (F) detected by qRT-PCR in c-MO and ahr2-MO-injected embryos compared with DMSO controls. Data represent 4 biological replicates analyzed by 2-way ANOVA with Tukey's *post hoc* test. Significantly different induction is designated with different letters ($P < .05$).

uniquely associated with the BEZO transcript profile (Fig. 6A). The next 2 most enriched biological networks, cell-matrix interactions and response to hypoxia and oxidative stress, were highly significant for both 7,12-B[a]AQ and BEZO. Iron transport

and protein folding-ER, and cytoplasm were also similarly significant with BEZO and 7,12-B[a]AQ exposures. By contrast, complement system, IL-6 signaling, and Kallikrein-Kinin system were more significantly enriched with 7,12-B[a]AQ

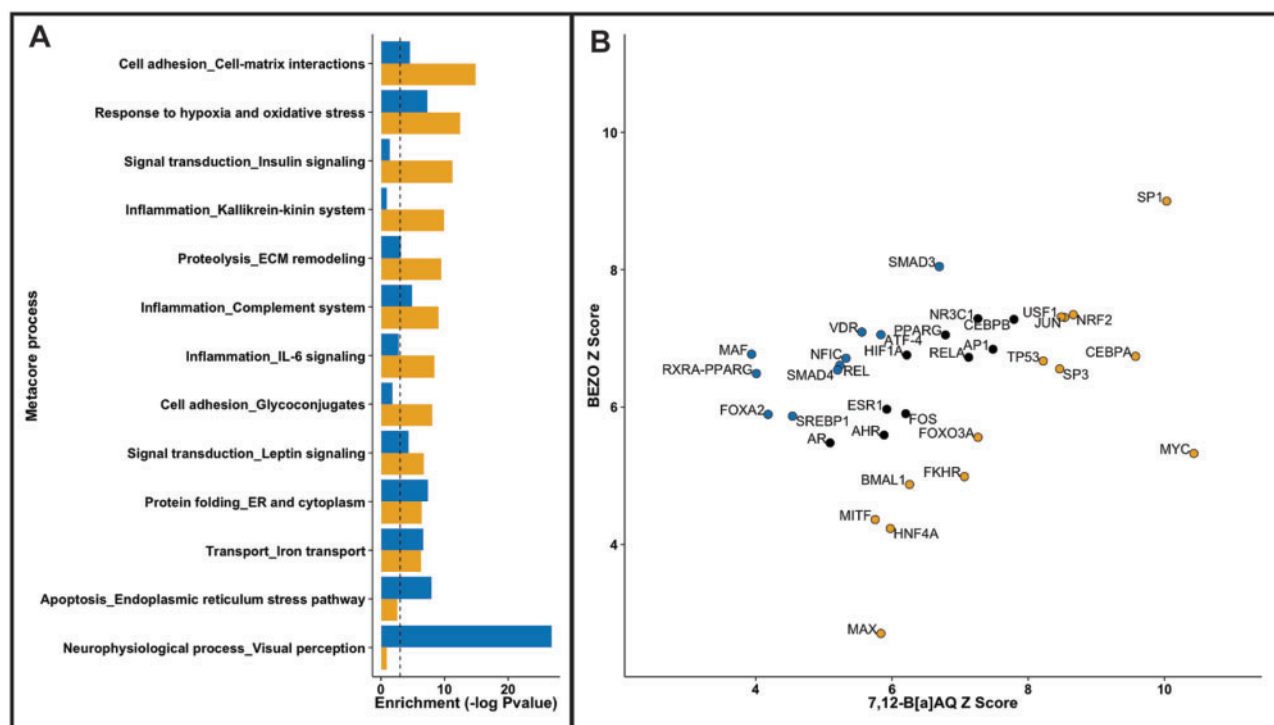


FIG. 6. Biological processes and transcriptional regulators affected by BEZO and 7,12-B[a]AQ exposure. A, MetaCore processes significantly over-represented among transcripts disrupted by BEZO and 7,12-B[a]AQ ($P < .001$). B, Transcriptional regulators significantly over-connected in BEZO or 7,12-B[a]AQ networks ($P < 5e-7$, Z score > 5). TFs with similar Z scores (difference < 1 between BEZO and 7,12-B[a]AQ) are indicated in black. TFs with higher Z scores for 7,12-B[a]AQ and BEZO are indicated with yellow and blue, respectively.

exposures, suggesting a more profound effect of 7,12-B[a]AQ on immune system development. The function of the individual members of these biological networks in developing zebrafish, and the role of the AHR in regulating their expression, awaits further investigation.

Multiple TFs Are Predicted to Regulate Gene Expression in BEZO and 7,12-B[a]AQ Exposed Developing Embryos

We used Metacore to identify 36 transcriptional hubs that are predicted to regulate significant networks of genes following BEZO or 7,12-B[a]AQ exposure ($P < 5.0e-7$, Z score > 5). We compared the Z scores of these TFs to identify regulatory hubs that could mediate the expression differences between the 2 OPAHs. The top predicted TFs, MYC and SP1, were significant for both OPAHs, but were more highly connected in the 7,12-B[a]AQ than the BEZO network (Fig. 6B, yellow). In addition to being identified as a regulatory hub, MYC transcript was significantly induced 1.4-fold by both 7,12-B[a]AQ and BEZO. The AHR cooperates with NfKB to induce MYC in mammary cells, and loss of AHR causes a decrease in MYC in mouse HSCs (Kim et al., 2000; Singh et al., 2014). NRF2, CEBPA, MAX, and JUN were similarly more connected in the 7,12-B[a]AQ than the BEZO network. None of them, however, were significantly DE at the transcript level.

NR2E3 (also known as photoreceptor-specific nuclear receptor) was uniquely significant in the BEZO network. MAF (v-maf avian musclaponeurotic fibrosarcoma oncogene homolog) and RXR-PPARG heterodimer, both of which are also involved in eye development, were significant for both OPAHs but were much more connected in the BEZO than the 7,12-B[a]AQ network (Fig. 6B, blue). This reflects the decreased expression of many visual system genes, including short and long wave opsins, gamma-

crystallins, visual system homeobox 1, retina, and anterior neural fold homeobox 1 in BEZO-exposed embryos (Supplementary Table S4). SMAD3, an important mediator of TGF β signaling and mesoderm formation in zebrafish, was also highly significant in the BEZO network. A third group of TFs, including AHR, AR, CEBPB, NR3C1 (Glucocorticoid receptor), NfKB subunit REL, AP1, and FOS, were similarly connected in the 2 OPAH networks (Fig. 6B, black, Z-score difference < 1). Expressions of CEBPB, AP1, and FOS transcripts were all increased > 1.4 -fold by both OPAHs. Many of these TFs interact and tightly coordinate responses to oxidative stress/redox homeostasis and other cellular functions.

Since we determined experimentally that both BEZO and 7,12-B[a]AQ-induced developmental toxicity depended on AHR2, we compared networks of known AHR interactors that were significantly DE > 1.5 -fold in BEZO and 7,12-B[a]AQ-exposed embryos (Fig. 7). Direction of expression change for each gene is indicated (red = up, blue = down, both colors displayed in cases of differing expression between homologs). The bicolor representation of AHR reflects differential expression of AHR homolog transcripts; *ahr2* was slightly increased in both 7,12-B[a]AQ and BEZO-exposed embryos. However, *ahr1b* was uniquely decreased 1.9-fold by BEZO. Both OPAHs increased expression of NFE2L1, CITED, and ATF, which are all TFs known to interact with AHR. BTEB (KLF9), which binds to GC boxes and regulates CYP1A expression, was decreased by both BEZO and 7,12-B[a]AQ (Imataka et al., 1992). A large group of AHR-interacting genes were unique to 7,12-B[a]AQ (Fig. 7, orange-shaded oval), and included FOXQ1 (Forced box Q1) which mediates TCDD-induced jaw malformations (Planchart and Mattingly, 2010). DB (leptin receptor), BACH, circadian rhythm effector Nocturnin, and TIE were other TFs induced by 7,12-B[a]AQ.

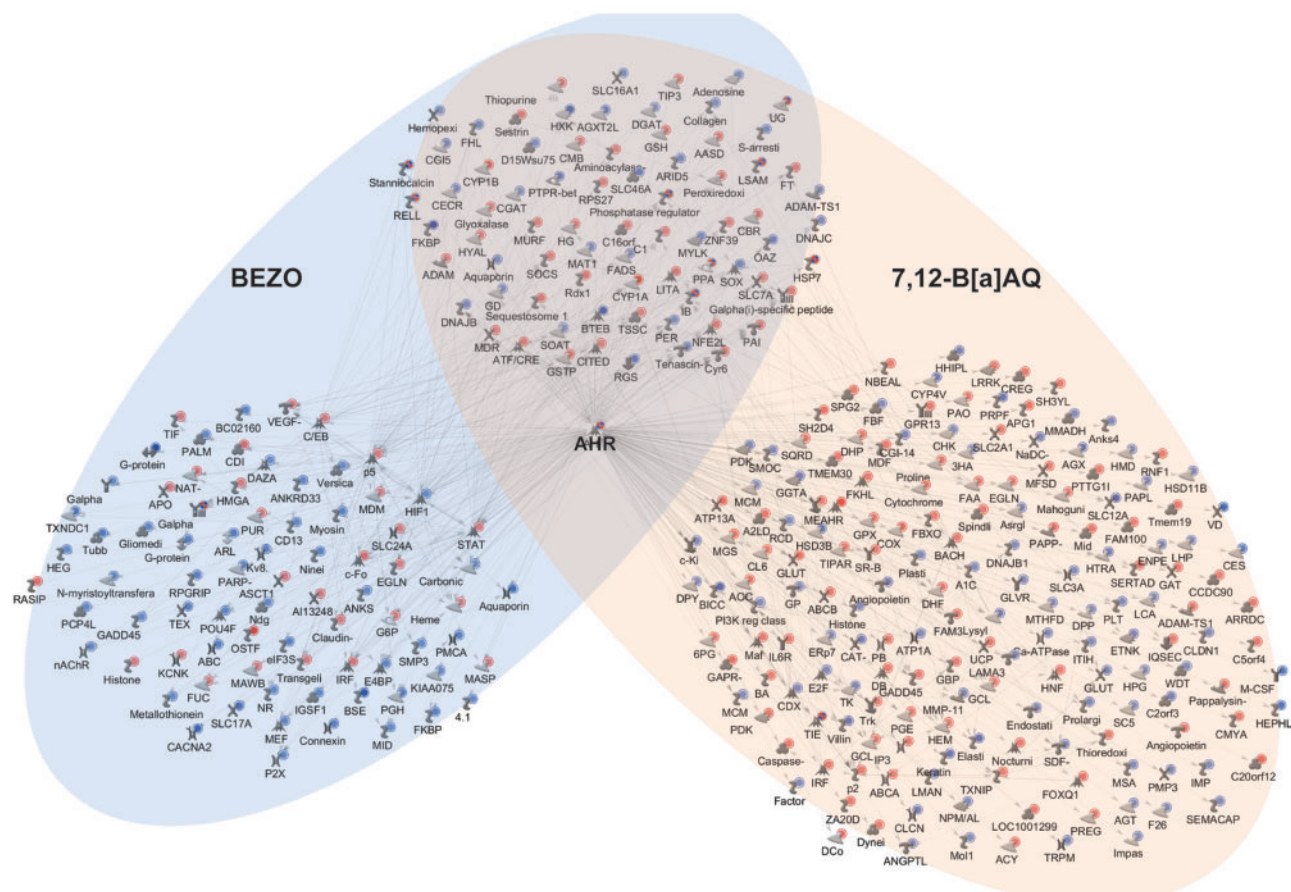


FIG. 7. DE genes in 7,12-B[a]AQ and BEZO exposed embryos include both overlapping and unique targets of the AHR. Predicted interactions between the AHR and transcripts DE following BEZO exposure are outlined in the blue shaded oval, 7,12-B[a]AQ transcripts are outlined in the orange shaded oval. Interactions were predicted using the Metacore statistical interactome tool. Color of circles represents expression of transcript compared with control (red = increased, blue = decreased).

AHR-interacting genes unique to BEZO-included TFs P53, C/EB, and STAT. HIF1 (*hif1a*) was significantly decreased. The induction of this cluster of TFs that interact with AHR may contribute to the severe, AHR2-dependent developmental toxicity of BEZO, despite its weak induction of canonical AHR target genes.

DISCUSSION

We investigated global transcriptional responses and the role of the AHR in mediating developmental toxicity of 2 OPAHs that occur in environmental samples. Despite their significant difference in Cyp1a induction and predicted AHR binding, we found that adverse developmental effects of both BEZO and 7,12-B[a]AQ are dependent on AHR2 in zebrafish. These OPAHs caused morphological abnormalities, including disrupted heart development, craniofacial abnormalities, eye defects, and edema, at comparable waterborne exposure concentrations. By analyzing transcriptional responses in developing zebrafish exposed to BEZO and 7,12-B[a]AQ, we identified gene expression profiles that indicate ligand-specific AHR signaling disrupts distinct biological processes that underlie developmental toxicity of these OPAHs.

While a difference in Cyp1a expression could be caused by many factors, such as uptake or pharmacokinetic distribution, our data suggest that receptor affinity is a primary driver of differences in gene expression between these compounds. Based on the similar log K_{ow} s of BEZO and 7,12-B[a]AQ (4.81 and 4.4,

respectively), we would not predict large differences in uptake (Meylan and Howard, 1995). In addition, BEZO and 7,12-B[a]AQ caused AHR2-dependent morphological abnormalities at a similar range of concentrations. We did not observe Cyp1a induction accompanying the first malformations observed at 48 hpf, nor did we observe differential timing of Cyp1a induction in BEZO-exposed embryos compared with 7,12-B[a]AQ. Both OPAHs were predicted to dock in an AHR receptor homology model (Table 1), but the binding energy was more favorable for 7,12-B[a]AQ docking with AHR2 than BEZO. This difference in binding with the AHR could result in ligand-specific activity, as has been shown with diverse AHR ligands (Soshilov and Denison, 2014). Differential regulation of downstream genes is further supported by our RNA-seq analysis, which provides new information on biological processes affected by OPAH exposure during development.

PAHs as AHR Ligands

A growing body of research shows that PAHs engage in complex interactions with the AHR, its coactivators, and other transcriptional regulators. Cyp1a protein expression and metabolic activity are widely used as biomarkers of AHR activation, as binding affinity of dioxin-like compounds and AHR-mediated toxicological effects have been demonstrated to correlate with CYP1A (Billiard et al., 2002). Compounds identified as AHR ligands are diverse, however, with some acting as partial agonists and/or antagonists. The structural diversity of parent PAH compounds,

substituted derivatives, and their propensity for metabolism further complicates prediction and interpretation of AHR interactions for this chemical class. Some 3-ring PAHs, such as fluoranthene, inhibit Cyp1a activity, though the mechanism by which these PAHs act as inhibitors remains unknown (Brown *et al.*, 2015; Willett *et al.*, 2001). This complexity can be visualized and mechanistically interrogated in zebrafish, where 4- and 5-ring PAH structures differentially interact with AHRs, resulting in tissue-specific Cyp1a expression patterns and a range of morphological effects (Incardona *et al.*, 2006, 2011; Knecht *et al.*, 2013). The malformations and Cyp1a expression profile we observed with 7,12-B[a]AQ are similar to effects previously observed with AHR agonists, including parent PAH BAA (Goodale *et al.*, 2013). The developmental toxicity and Cyp1a activation profile of BEZO, however, is unlike previously described AHR agonists or antagonists.

Because of its use in dye manufacture and associated reports of dermal lesions and decreased liver function in exposed workers, several studies have investigated BEZO toxicity in rodents. Exposure to high concentrations of BEZO causes liver, kidney, and testis histopathological changes in guinea pigs, which is attenuated with ascorbic acid supplementation (Das *et al.*, 1994). Singh *et al.* (2003) observed decreased cytochrome P-450 phase 1 enzymes and ethoxresorufin-O-deethylase activity in guinea pigs exposed to BEZO. Both in that study and others, BEZO caused a decrease in glutathione (GSH), and an increase in cytochrome P-450 phase 2 enzymes including glutathione peroxidase and glutathione reductase (Dwivedi *et al.*, 2001). To our knowledge, involvement of the AHR in these effects awaits investigation. In agreement with previous studies, we observed an increase in phase 2 metabolizing enzymes, and we additionally demonstrated that BEZO induction of *gstp2* was AHR2 dependent.

Studies with AHR agonists and alternative AHR ligands, both in cell culture and animal models, have recently highlighted how ligands can differentially mediate AHR-dependent biological processes. Several selective AHR modulators (SAhRMs) have been identified, which do not induce canonical AHR signaling such as CYP1A expression but bind the receptor and repress inflammatory signaling (Narayanan *et al.*, 2012). AHR-mediated responses in the absence of a xenobiotic ligand, including both *cyp1a* induction in hyperoxia, as well as decreased *cyp1a* expression resulting from oxidative stress have also been reported (Barker *et al.*, 1994; Couroucli *et al.*, 2002). In this context, an environmentally relevant OPAH that induces AHR-dependent developmental toxicity in the absence of strong Cyp1a expression is not entirely unexpected.

Differential Regulation of Canonical AHR Targets and Phase 2 Metabolism

We used RNA-seq to compare gene expression profiles induced by BEZO and 7,12-B[a]AQ. Their 60-fold difference in *cyp1a* mRNA induction lead us to anticipate that global gene expression differences could illuminate mechanisms that lead to their similar downstream effects on phenotype. We found that *cyp1c1*, *cyp1c2*, *cyp1b1*, *ahrrb*, and *wfikkn1* were also more highly induced by 7,12-B[a]AQ than BEZO. These transcripts are known targets of the AHR, which are similarly induced by BAA (Goodale *et al.*, 2013; Jonsson *et al.*, 2007). Other transcripts associated with AHR activation, however, were elevated at comparable levels by BEZO and 7,12-B[a]AQ. These included oxidative stress-related and phase 2 metabolizing enzymes *gsr*, *prdx1*, and *sult6b1*. We additionally identified a large group of transcripts

related to eye development that were more strongly affected by BEZO than 7,12-B[a]AQ.

Many transcripts that changed in response to these PAHs are not known to be direct targets of the AHR, but are regulated via other TFs, such as the antioxidant response element TF NFE2 p45-related 2 (NRF2), that crosstalk with AHR (Tian *et al.*, 1999; Timme-Laragy *et al.*, 2009). Several NRF family TFs, which regulate genes that protect the cell from oxidative damage, have dioxin responsive elements and can be induced directly by the AHR (Timme-Laragy *et al.*, 2009). Some pathways induced by these OPAHs therefore protect the embryo from damage (Van Tiem and Di Giulio, 2011). Repression of Cyp1a expression via chemical or morpholino inhibition can exacerbate the AHR-mediated toxicity of PAHs, leading to increased oxidative stress. The AHR-mediated effects of BEZO could potentially be amplified as a result of simultaneous Cyp1a inhibition.

While both OPAHs induced expression of oxidative stress response genes including *gsr*, *gstp1*, *prdx1*, and *nfe2l1*, the BEZO-specific genes and biological processes suggest additional uncoupling of redox reactions. Arginase 2 (*arg2*), which was increased only by BEZO, is an important regulator of nitric oxide production. Excessive *arg2* activity can be driven by reactive oxygen species (ROS), and is associated with cardiovascular disease, vascular structure problems, neural toxicity, and retinopathy (Caldwell *et al.*, 2015; Durante, 2013). Oxidative stress and disruption of AHR/ARNT signaling have both been associated with visual system disruption, and an isoform of the AHR repressor (*ahrra*) was recently shown to be important for photoreceptor development in zebrafish (Aluru *et al.*, 2014). We investigated AHR2 dependence of *arg2* and *igfbp1a*, which were highly DE by BEZO, to see whether transcripts unique to this OPAH were disrupted independently of AHR2. We found no evidence of AHR2-independent regulation. However, we identified *arg2*, and *igfbp1a* as AHR2-dependent transcripts elevated more highly by BEZO than 7,12-B[a]AQ, which may mediate BEZO-specific effects on development.

Predicting Ligand-Specific Interactions With TFs and Co-Activators

Our network analysis of DE genes indicated that BEZO and 7,12-B[a]AQ favored differential interactions between the AHR and other transcriptional regulators or co-activators. As a member of the PAS family of TFs, the AHR interacts with other PAS proteins and shares the requirement of the AHR nuclear translocator (ARNT) for dimerization and transcriptional activation with HIF1A (Gu *et al.*, 2000). AHR crosstalk via other binding partners and co-activators, including p300 (CREB binding protein), HSP90, the AHR repressor (AHRR) and JUN have been reported (Beischlag *et al.*, 2008; Evans *et al.*, 2008). Tan *et al.* (2002) found that MAPK8 (JNK) interaction with ARNT potentiated TCDD induction of CYP1A. SP600125, which we compared here with BEZO and 7,12-B[a]AQ for predicted AHR binding affinity, is a weak AHR agonist that was originally identified as a potent inhibitor of JNK (Dvorak *et al.*, 2008). JNKs are important regulators of embryonic eye development, and SP600125 was found to induce developmental aberrations in zebrafish embryos similar to BEZO (Huang *et al.*, 2013; Valesio *et al.*, 2013). The identification of SP600125 and other MAP kinase inhibitors as weak AHR agonists highlights the idea that chemicals can bind multiple interacting proteins. The unusual AHR activation profile of BEZO could similarly result from interaction with multiple targets.

OPAHs likely interact with cells in a multitude of ways, by binding receptors, increasing ROS, and causing DNA and/or

protein damage. The dependence of both BEZO and 7,12-B[a]A-induced developmental toxicity on AHR2 is therefore striking. Confirming the involvement of predicted TFs and interacting proteins will be an important direction for future studies, and further investigation will be necessary to elucidate noncanonical AHR2 signaling pathways in the developing embryo. Comparative transcriptional profiling demonstrates that OPAH induction of canonical AHR regulated genes correlates with predicted affinity for the receptor, but ligand-specific AHR interactions affect other signaling pathways that mediate developmental toxicity. Our studies highlight the importance of considering biomarkers of AHR activation beyond Cyp1a, and investigating mechanisms of diverse PAH structures. We identified clusters of transcripts associated with OPAHs that induce AHR-dependent toxicity. Deeper characterization of the AHR interactome will catalyze predictive capability for this diverse group of environmentally relevant chemicals.

FUNDING

National Institutes of Health NIEHS Superfund Research Program (P42 ES016465), Core Center Grant (P30 ES000210), and the NIEHS Training Grant (T32 ES007060). Pacific Northwest National Laboratory is a multi-program national laboratory operated by Battelle Memorial Institute for the DOE under contract number DE-AC05-76RLO1830.

SUPPLEMENTARY DATA

Supplementary data are available online at <http://toxsci.oxfordjournals.org/>.

ACKNOWLEDGMENTS

The authors thank Cari Buchner, Carrie Barton, Annika Swanson, and the staff at the Sinnhuber Aquatic Research Laboratory for their excellent fish husbandry and assistance with OPAH exposures. We also thank Lisa Truong, Jill Franzosa, and Derik Haggard for advice with RNA-seq analysis and critical review of the manuscript. Jason Carriere processed the RNA samples and conducted mRNA sequencing at the University of Oregon Genomics Core Facility, Eugene, Oregon. The cyp1a reporter line, Tg(cyp1a:nls-egfp) was a kind gift from Professor Seok-Yong Choi, Chonnam National University Medical School Gwangju, Republic of Korea. We thank OSU Superfund Research Program Core D/Anderson Laboratory for their analytical support and providing OPAHs.

REFERENCES

- Aluru, N., Jenny, M. J., and Hahn, M. E. (2014). Knockdown of a zebrafish aryl hydrocarbon receptor repressor (AHRRA) affects expression of genes related to photoreceptor development and hematopoiesis. *Toxicol. Sci.* **139**, 381–395.
- Anders, S., Pyl, P. T., and Huber, W. (2014). HTSeq—a python framework to work with high-throughput sequencing data. *Bioinformatics* **31**, 166–169.
- Barker, C. W., Fagan, J. B., and Pasco, D. S. (1994). Down-regulation of P4501A1 and P4501A2 mRNA expression in isolated hepatocytes by oxidative stress. *J. Biol. Chem.* **269**, 3985–3990.
- Beischlag, T. V., Luis Morales, J., Hollingshead, B. D., and Perdew, G. H. (2008). The aryl hydrocarbon receptor complex and the control of gene expression. *Crit. Rev. Eukaryot. Gene Expr.* **18**, 207–250.
- Billiard, S. M., Hahn, M. E., Franks, D. G., Peterson, R. E., Bols, N. C., and Hodson, P. V. (2002). Binding of polycyclic aromatic hydrocarbons (PAHs) to teleost aryl hydrocarbon receptors (AHRs). *Comp. Biochem. Physiol. B Biochem. Mol. Biol.* **133**, 55–68.
- Bostrom, C. E., Gerde, P., Hanberg, A., Jernstrom, B., Johansson, C., Kyrklund, T., Rannug, A., Tornqvist, M., Victorin, K., and Westerholm, R. (2002). Cancer risk assessment, indicators, and guidelines for polycyclic aromatic hydrocarbons in the ambient air. *Environ. Health Perspect.* **110**(Suppl 3), 451–488.
- Brown, D. R., Clark, B. W., Garner, L. V. T., and Di Giulio, R. T. (2015). Zebrafish cardiotoxicity: the effects of CYP1A inhibition and AHR2 knockdown following exposure to weak aryl hydrocarbon receptor agonists. *Environ. Sci. Pollut. Res. Int.* **22**, 8329–8338.
- Caldwell, R. B., Toque, H. A., Narayanan, S. P., and Caldwell, R. W. (2015). Arginase: an old enzyme with new tricks. *Trends Pharmacol. Sci.* **36**, 395–405.
- Carney, S. A., Peterson, R. E., and Heideman, W. (2004). 2,3,7,8-Tetrachlorodibenzo-p-dioxin activation of the Aryl hydrocarbon receptor/aryl hydrocarbon receptor nuclear translocator pathway causes developmental toxicity through a CYP1A-independent mechanism in zebrafish. *Mol. Pharmacol.* **66**, 512–521.
- Courouclis, X. I., Welty, S. E., Geske, R. S., and Moorthy, B. (2002). Regulation of pulmonary and hepatic cytochrome P4501A expression in the rat by hyperoxia: implications for hyperoxic lung injury. *Mol. Pharmacol.* **61**, 507–515.
- Das, M., Garg, K., Singh, G. B., and Khanna, S. K. (1994). Attenuation of benzanthrone toxicity by ascorbic acid in guinea pigs. *Fund. Appl. Toxicol.* **22**, 447–456.
- Durant, J. L., Busby, W. F., Jr., Lafleur, A. L., Penman, B. W., and Crespi, C. L. (1996). Human cell mutagenicity of oxygenated, nitrated and unsubstituted polycyclic aromatic hydrocarbons associated with urban aerosols. *Mutat. Res.* **371**, 123–157.
- Durante, W. (2013). Role of arginase in vessel wall remodeling. *Front. Immunol.* **4**, 111.
- Dvorak, Z., Vrzal, R., Henklova, P., Jancova, P., Anzenbacherova, E., Maurel, P., Svecova, L., Pavsek, P., Ehrmann, J., Havlik, R., et al. (2008). JNK inhibitor SP600125 is a partial agonist of human aryl hydrocarbon receptor and induces CYP1A1 and CYP1A2 genes in primary human hepatocytes. *Biochem. Pharmacol.* **75**, 580–588.
- Dwivedi, N., Das, M., and Khanna, S. K. (2001). Role of biological antioxidants in benzanthrone toxicity. *Arch. Toxicol.* **75**, 221–226.
- USEPA (2015). National Waste Minimization Program. <http://www.epa.gov/osw/hazard/wastemin/priority.htm>. Accessed May 5, 2015.
- Evans, B. R., Karchner, S. I., Allan, L. L., Pollenz, R. S., Tanguay, R. L., Jenny, M. J., Sherr, D. H., and Hahn, M. E. (2008). Repression of aryl hydrocarbon receptor (AHR) signaling by AHR repressor: role of DNA binding and competition for AHR nuclear translocator. *Mol. Pharmacol.* **73**, 387–398.
- Gerlach, C. V., Das, S. R., Volz, D. C., Bisson, W. H., Kolluri, S. K., and Tanguay, R. L. (2014). Mono-substituted isopropylated triaryl phosphate, a major component of Firemaster 550, is an AHR agonist that exhibits AHR-independent cardiotoxicity in zebrafish. *Aquat. Toxicol.* **154**, 71–79.
- Goodale, B. C., Tilton, S. C., Corvi, M. M., Wilson, G. R., Janszen, D. B., Anderson, K. A., Waters, K. M., and Tanguay, R. L. (2013). Structurally distinct polycyclic aromatic hydrocarbons

- induce differential transcriptional responses in developing zebrafish. *Toxicol. Appl. Pharmacol.* **272**, 656–670.
- Gu, Y. Z., Hogenesch, J. B., and Bradfield, C. A. (2000). The PAS superfamily: sensors of environmental and developmental signals. *Annu. Rev. Pharmacol. Toxicol.* **40**, 519–561.
- Huang, L., Wang, C., Zhang, Y., Wu, M., and Zuo, Z. (2013). Phenanthrene causes ocular developmental toxicity in zebrafish embryos and the possible mechanisms involved. *J. Hazard. Mater.* **261**, 172–180.
- Imataka, H., Sogawa, K., Yasumoto, K., Kikuchi, Y., Sasano, K., Kobayashi, A., Hayami, M., and Fujii-Kuriyama, Y. (1992). Two regulatory proteins that bind to the basic transcription element (BTE), a GC box sequence in the promoter region of the rat P-4501A1 gene. *EMBO J.* **11**, 3663–3671.
- Incardona, J. P., Day, H. L., Collier, T. K., and Scholz, N. L. (2006). Developmental toxicity of 4-ring polycyclic aromatic hydrocarbons in zebrafish is differentially dependent on AH receptor isoforms and hepatic cytochrome P4501A metabolism. *Toxicol. Appl. Pharmacol.* **217**, 308–321.
- Incardona, J. P., Linbo, T. L., and Scholz, N. L. (2011). Cardiac toxicity of 5-ring polycyclic aromatic hydrocarbons is differentially dependent on the aryl hydrocarbon receptor 2 isoform during zebrafish development. *Toxicol. Appl. Pharmacol.* **257**, 242–249.
- Jonsson, M. E., Jenny, M. J., Woodin, B. R., Hahn, M. E., and Stegeman, J. J. (2007). Role of AHR2 in the expression of novel cytochrome P450 1 family genes, cell cycle genes, and morphological defects in developing zebra fish exposed to 3,3',4,4',5-pentachlorobiphenyl or 2,3,7,8-tetrachlorodibenzo-p-dioxin. *Toxicol. Sci.* **100**, 180–193.
- Kim, D. W., Gazourian, L., Quadri, S. A., Romieu-Mourez, R., Sherr, D. H., and Sonenshein, G. E. (2000). The RelA NF- κ B subunit and the aryl hydrocarbon receptor (AhR) cooperate to transactivate the c-myc promoter in mammary cells. *Oncogene* **19**, 5498–5506.
- Kim, K.-H., Park, H.-J., Kim, J. H., Kim, S., Williams, D. R., Kim, M.-K., Jung, Y. D., Teraoka, H., Park, H.-C., Choy, H. E., et al. (2013). Cyp1a reporter zebrafish reveals target tissues for dioxin. *Aquat. Toxicol.* **134–135**, 57–65.
- Kimmel, C. B., Ballard, W. W., Kimmel, S. R., Ullmann, B., and Schilling, T. F. (1995). Stages of embryonic development of the zebrafish. *Dev. Dyn.* **203**, 253–310.
- Knecht, A. L., Goodale, B. C., Truong, L., Simonich, M. T., Swanson, A. J., Matzke, M. M., Anderson, K. A., Waters, K. M., and Tanguay, R. L. (2013). Comparative developmental toxicity of environmentally relevant oxygenated PAHs. *Toxicol. Appl. Pharmacol.* **271**, 266–275.
- Lanham, K. A., Plavicki, J., Peterson, R. E., and Heideman, W. (2014). Cardiac myocyte-specific AHR activation phenocopies TCDD-induced toxicity in zebrafish. *Toxicol. Sci.* **141**, 141–154.
- Layshock, J. A., Wilson, G., and Anderson, K. A. (2010). Ketone and quinone-substituted polycyclic aromatic hydrocarbons in mussel tissue, sediment, urban dust, and diesel particulate matrices. *Environ. Toxicol. Chem.* **29**, 2450–2460.
- Lundstedt, S., Persson, Y., and Oberg, L. (2006). Transformation of PAHs during ethanol-Fenton treatment of an aged gasworks' soil. *Chemosphere* **65**, 1288–1294.
- Lundstedt, S., White, P. A., Lemieux, C. L., Lynes, K. D., Lambert, I. B., Oberg, L., Haglund, P., and Tysklind, M. (2007). Sources, fate, and toxic hazards of oxygenated polycyclic aromatic hydrocarbons (PAHs) at PAH-contaminated sites. *Ambio* **36**, 475–485.
- Mbewe-Campbell, N., Wei, Z., Zhang, K., Friese, R. S., Mahata, M., Schork, A. J., Rao, F. et al. (2012). Genes and Environment: Novel, Functional Polymorphism in the Human Cathepsin L (CTSL1) Promoter Disrupts a Xenobiotic Response Element (XRE) to Alter Transcription and Blood Pressure. *J. Hypertens* **30**, 1961–1969.
- Meylan, W. M., and Howard, P. H. (1995). Atom fragment contribution method for estimating octanol-water partition-coefficients. *J. Pharm. Sci.* **84**, 83–92.
- Narayanan, G. A., Murray, I. A., Krishnegowda, G., Amin, S., and Perdew, G. H. (2012). Selective aryl hydrocarbon receptor modulator-mediated repression of CD55 expression induced by cytokine exposure. *J. Pharmacol. Exp. Ther.* **342**, 345–355.
- Nielsen, T., Feilberg, A., and Binderup, M. L. (1999). The variation of street air levels of PAH and other mutagenic PAC in relation to regulations of traffic emissions and the impact of atmospheric processes. *Environ. Sci. Pollut. Res.* **6**, 133–137.
- Nikolsky, Y., Kirillov, E., Zuev, R., Rakhmatulin, E., and Nikolskaya, T. (2009). Functional analysis of OMICS data and small molecule compounds in an integrated 'knowledge-based' platform. *Methods Mol. Biol.* **563**, 177–196.
- Perkins, A., Phillips, J. L., Kerkvliet, N. I., Tanguay, R. L., Perdew, G. H., Kolluri, S. K., and Bisson, W. H. (2014). A structural switch between agonist and antagonist bound conformations for a ligand-optimized model of the human aryl hydrocarbon receptor ligand binding domain. *Biology (Basel)* **3**, 645–669.
- Pfaffl, M. W. (2001). A new mathematical model for relative quantification in real-time RT-PCR. *Nucleic Acids Res.* **29**, e45.
- Planchart, A., and Mattingly, C. J. (2010). 2,3,7,8-Tetrachlorodibenzo-p-dioxin upregulates FoxQ1b in zebrafish jaw primordium. *Chem. Res. Toxicol.* **23**, 480–487.
- Ramirez, N., Cuadras, A., Rovira, E., Marce, R. M., and Borrell, F. (2011). Risk assessment related to atmospheric polycyclic aromatic hydrocarbons in gas and particle phases near industrial sites. *Environ. Health Perspect.* **119**, 1110–1116.
- Reimers, M. J., La Du, J. K., Piera, C. B., Giovanini, J., and Tanguay, R. L. (2006). Ethanol-dependent toxicity in zebrafish is partially attenuated by antioxidants. *Neurotoxicol. Teratol.* **28**, 497–508.
- Robinson, M. D., McCarthy, D. J., and Smyth, G. K. (2010). edgeR: a bioconductor package for differential expression analysis of digital gene expression data. *Bioinformatics* **26**, 139–140.
- Shannon, P., Markiel, A., Ozier, O., Baliga, N. S., Wang, J. T., Ramage, D., Amin, N., Schwikowski, B., and Ideker, T. (2003). Cytoscape: a software environment for integrated models of biomolecular interaction networks. *Genome Res.* **13**, 2498–2504.
- Singh, K. P., Bennett, J. A., Casado, F. L., Walrath, J. L., Welle, S. L., and Gasiewicz, T. A. (2014). Loss of aryl hydrocarbon receptor promotes gene changes associated with premature hematopoietic stem cell exhaustion and development of a myeloproliferative disorder in aging mice. *Stem Cells Dev.* **23**, 95–106.
- Singh, R. P., Khanna, R., Kaw, J. L., Khanna, S. K., and Das, M. (2003). Comparative effect of benzantrone and 3-bromobenzanthrone on hepatic xenobiotic metabolism and anti-oxidative defense system in guinea pigs. *Arch. Toxicol.* **77**, 94–99.
- Soshilov, A. A., and Denison, M. S. (2014). Ligand promiscuity of aryl hydrocarbon receptor agonists and antagonists revealed by site-directed mutagenesis. *Mol. Cell. Biol.* **34**, 1707–1719.
- Svedman, C., Zimerson, E., and Bruze, M. (2014). Allergic contact dermatitis caused by benzantrone in a pair of trousers. *Contact Dermatitis* **71**, 54–57.

- Svoboda, K. R., Linares, A. E., and Ribera, A. B. (2001). Activity regulates programmed cell death of zebrafish Rohon-Beard neurons. *Development* **128**, 3511–3520.
- Tan, Z., Chang, X., Puga, A., and Xia, Y. (2002). Activation of mitogen-activated protein kinases (MAPKs) by aromatic hydrocarbons: role in the regulation of aryl hydrocarbon receptor (AHR) function. *Biochem. Pharmacol.* **64**, 771–780.
- Tewari, P., Roy, R., Mishra, S., Mandal, P., Yadav, A., Chaudhari, B. P., Chaturvedi, R. K., Dwivedi, P. D., Tripathi, A., and Das, M. (2015). Benzanthrone induced immunotoxicity via oxidative stress and inflammatory mediators in Balb/c mice. *Immunobiology* **220**, 369–381.
- Tian, Y., Ke, S., Denison, M. S., Rabson, A. B., and Gallo, M. A. (1999). Ah receptor and NF-kappaB interactions, a potential mechanism for dioxin toxicity. *J. Biol. Chem.* **274**, 510–515.
- Tilton, S. C., Tal, T. L., Scroggins, S. M., Franzosa, J. A., Peterson, E. S., Tanguay, R. L., and Waters, K. M. (2012). Bioinformatics resource manager v2.3: an integrated software environment for systems biology with microRNA and cross-species analysis tools. *BMC Bioinformatics* **13**, 311.
- Timme-Laragy, A. R., Van Tiem, L. A., Linney, E. A., and Di Giulio, R. T. (2009). Antioxidant responses and NRF2 in synergistic developmental toxicity of PAHs in zebrafish. *Toxicol. Sci.* **109**, 217–227.
- Trapnell, C., Pachter, L., and Salzberg, S. L. (2009). TopHat: discovering splice junctions with RNA-Seq. *Bioinformatics* **25**, 1105–1111.
- Truong, L., Harper, S. L., and Tanguay, R. L. (2011). Evaluation of embryotoxicity using the zebrafish model. *Methods Mol. Biol.* **691**, 271–279.
- Valesio, E. G., Zhang, H., and Zhang, C. (2013). Exposure to the JNK inhibitor SP600125 (anthrapyrazolone) during early zebrafish development results in morphological defects. *J. Appl. Toxicol.* **33**, 32–40.
- Van Tiem, L. A., and Di Giulio, R. T. (2011). AHR2 knockdown prevents PAH-mediated cardiac toxicity and XRE- and ARE-associated gene induction in zebrafish (*Danio rerio*). *Toxicol. Appl. Pharmacol.* **254**, 280–287.
- Walgraeve, C., Demeestere, K., Dewulf, J., Zimmermann, R., and Van Langenhove, H. (2010). Oxygenated polycyclic aromatic hydrocarbons in atmospheric particulate matter: molecular characterization and occurrence. *Atmos. Environ.* **44**, 1831–1846.
- Wang, W., Jariyasopit, N., Schrlau, J., Jia, Y., Tao, S., Yu, T. W., Dashwood, R. H., Zhang, W., Wang, X., and Simonich, S. L. (2011). Concentration and photochemistry of PAHs, NPAHs, and OPAHs and toxicity of PM2.5 during the Beijing Olympic Games. *Environ. Sci. Technol.* **45**, 6887–6895.
- Wei, S. L., Huang, B., Liu, M., Bi, X. H., Ren, Z. F., Sheng, G. Y., and Fu, J. M. (2012). Characterization of PM2.5-bound nitrated and oxygenated PAHs in two industrial sites of South China. *Atmos. Res.* **109**, 76–83.
- Willett, K. L., Wassenberg, D., Lienesch, L., Reichert, W., and Di Giulio, R. T. (2001). In vivo and in vitro inhibition of CYP1A-dependent activity in *Fundulus heteroclitus* by the polynuclear aromatic hydrocarbon fluoranthene. *Toxicol. Appl. Pharmacol.* **177**, 264–271.
- Young, M. D., Wakefield, M. J., Smyth, G. K., and Oshlack, A. (2010). Gene ontology analysis for RNA-seq: accounting for selection bias. *Genome Biol.* **11**, R14.